Electronic Supplementary Material (ESI) for Physical Chemistry Chemical Physics.

Supporting Information

Modulating Carrier Dynamics through Perovskite Film Engineering

Swee Sien Lim[1,2], Wee Kiang Chong [1,2], Ankur Solanki[2], Herlina Arianita Dewi[3], Subodh Mhaisalkar[3,4], Nripan Mathews[3,4]†, and Tze Chien Sum[2]†

[1] Energy Research Institute @NTU (ERI@N), Interdisciplinary Graduate School Nanyang Technological University, Singapore

[2] School of Physical and Mathematical Sciences, Nanyang Technological University, 21 Nanyang Link, 637371, Singapore

[3] Energy Research Institute @NTU (ERI@N), Research Techno Plaza, X-Frontier Block, Level 5, 50 Nanyang Drive, Singapore 637553

[4] School of Materials Science and Engineering Nanyang Technological University Nanyang Avenue, 639798, Singapore

Corresponding Author

†Email: Tzechien@ntu.edu.sg (T.C.S), Nripan@ntu.edu.sg (N.M.)

KEYWORDS: $CH_3NH_3PbI_3$, film engineering, morphology, charge dynamics, trap density, diffusion lengths

Experimental Section

Thin film synthesis. A standard method is used to prepare a perovskite solution for perovskite spincoating. 78.3 mg/ml lead(II) iodide (Acros Organics PbI_2) and 27.0 mg/ml methylammonium iodide (DyeSol CH_3NH_3I) was dissolved in N,N-Dimethylformamide (Sigma Aldrich DMF) in a N_2-filled glovebox to obtain a clear yellow 10 wt. % methylammonium lead iodide ($CH_3NH_3PbI_3$) solution. Neat perovskite films were obtained by single-step deposition by spin-coating the

heated solution (70 ^{o}C) onto cleaned 1 mm-thick quartz substrates at 2000 RPM for 60 seconds and annealed at 100 ^{o}C for 30 minutes. For the substrate modification, the substrates were either cleaned with air-plasma for 10 minutes or etched with piranha solution (3 parts of concentrated H_2SO_4 to 1 part of H_2O_2) for 30 minutes, rinsed with de-ionised water and dried. The thin film modification was performed during the spin-coating process, where toluene (3 parts of toluene for 1 part of $CH_3NH_3PbI_3$ solution) was dripped 5 seconds into the start of the spin-coating. To maintain atmospheric and humidity integrity for optical spectroscopy, samples were mounted in a sample holder that was transferred into the glovebox and then sealed.

Experimental methods. The XRD spectra of the perovskite films were measured with a Bruker A8 Advance X-Ray diffractometer (Cu Kα, λ=1.5406Å). SEM images were obtained using a JEOL JSM6700F field emission scanning electron microscope. AFM images were obtained using an Asylum Research MFP-3D AFM system in tapping mode. Time-resolved and steady-state photoluminescence were performed in a backscattering geometry with an excitation wavelength of 600 nm. A Coherent OPerA Solo optical parametric amplifier pumped with a Coherent Libra™ regenerative amplifier (50 fs, 1KHz, 800 nm) was used to generate the excitation wavelength. The steady state photoluminescence was collected at an angle of ~150° by a collimating lens pair and collected by a fibre coupled to an Acton Spectra Pro 2500i spectrometer with a Princeton Instruments PIXIS 400B CCD camera. For time-resolved photoluminescence, the emission was collected by an Acton Spectra Pro 2300i monochromator coupled to an Optronis Optoscope™ streak camera, which has a temporal resolution of ~10 ps. Femtosecond pump-probe experiments were performed with an Ultrafast Systems HELIOS Femtosecond Transient Absorption Spectrometer and a home-built setup. For the HELIOS, a Coherent Legend™

regenerative amplifier (150 fs, 1KHz, 800 nm) seeded by a Coherent Vitesse™ oscillator (100 fs, 80 MHz) was used for white-light continuum and pump generation with a Coherent TOPAS-C optical parametric amplifier to generate the 600 nm pump beam which was chopped at 500 Hz. A 750 nm short pass filter was placed in the probe arm before the sample to attenuate the 800 nm fundamental beam used for WLC generation. For the home-built setup, the Libra (to generate the white-light continuum) and OPerA-Solo was used.

Characterization results

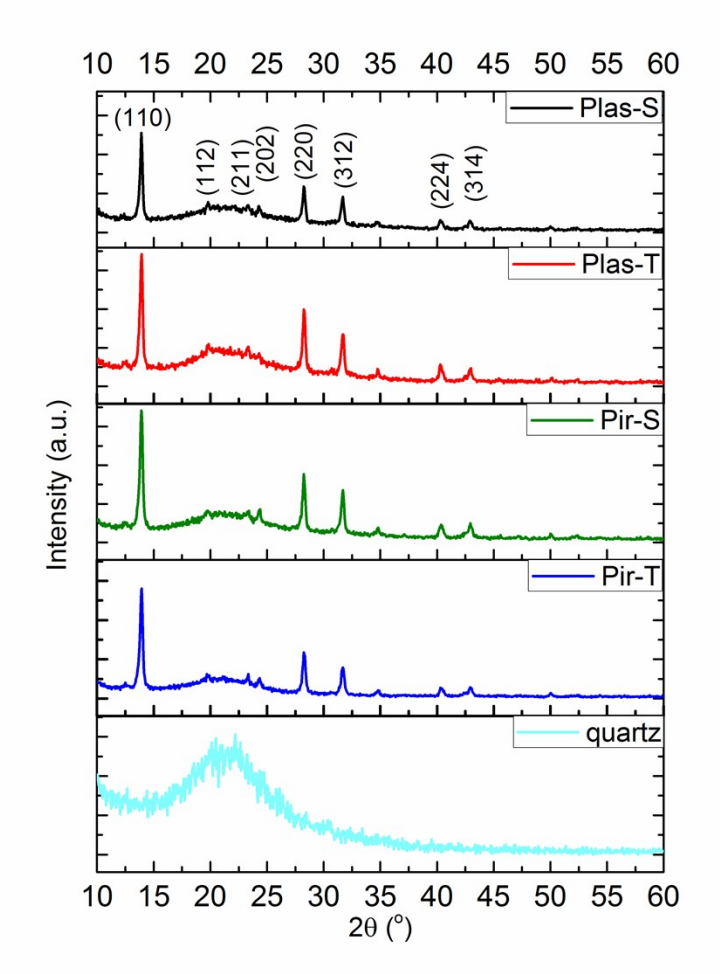

Figure S1. XRD spectra of the perovskite samples with different treatments: (a) Plas-S, (b) Plas-T, (c) Pir-S, and (d) Pir-T, and (e) quartz

Figure S1 shows the XRD spectra of the perovskite samples and a reference quartz substrate. As observed from Figure S1(a)-(d), the various treatments do not affect the perovskite crystallinity. There is also minimal amount of PbI_2 phase present in the spincoated films, evident from the weak peak at 12.5°.

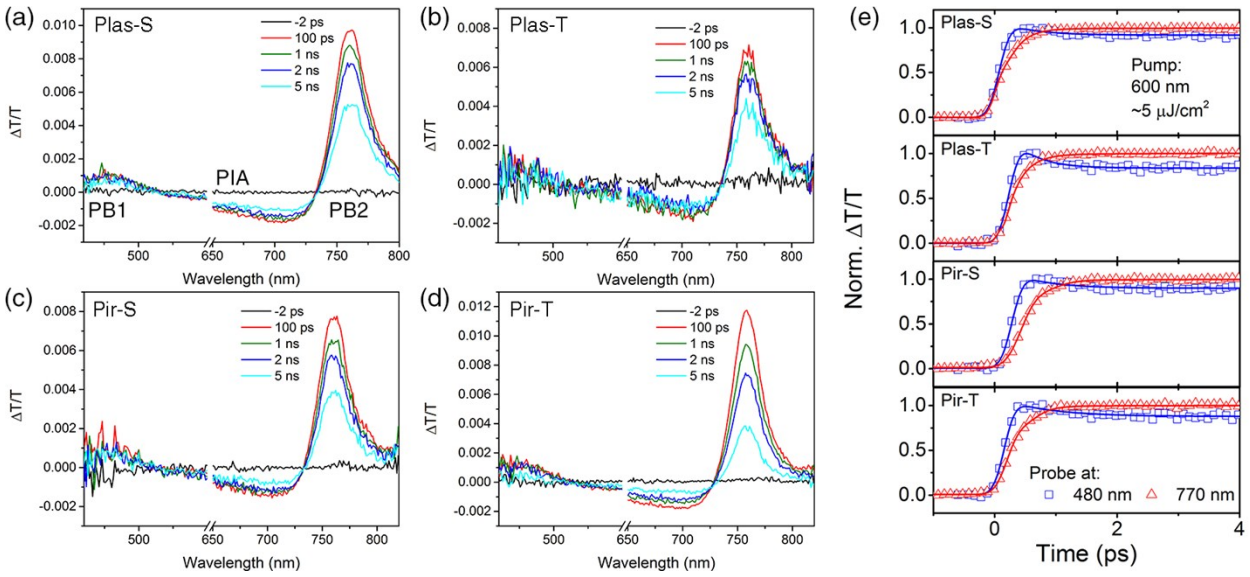

Figure S2. TA (a-d) spectra and (e) early time kinetics of the perovskite samples with different treatments (a) Plas-S, (b) Plas-T, (c) Pir-S, and (d) Pir-T at different time delays after 600 nm photoexcitation with a fluence of 5 μJ cm^{-2}.

Figure S2(a-d) shows the TA spectra of the perovskite samples in the visible regime across different time delays after photoexcitation by a 600 nm pump pulse with a fluence of 5 μJ cm^{-2} and probed by a white-light continuum. The characteristic photobleaching bands centered at ~480 nm and ~760 nm, and the broad photoinduced absorption band can be seen in all samples. The early time kinetics (Figure S2e) suggests that hot carrier cooling is still present (crossing of 480 nm and 770 nm trace).

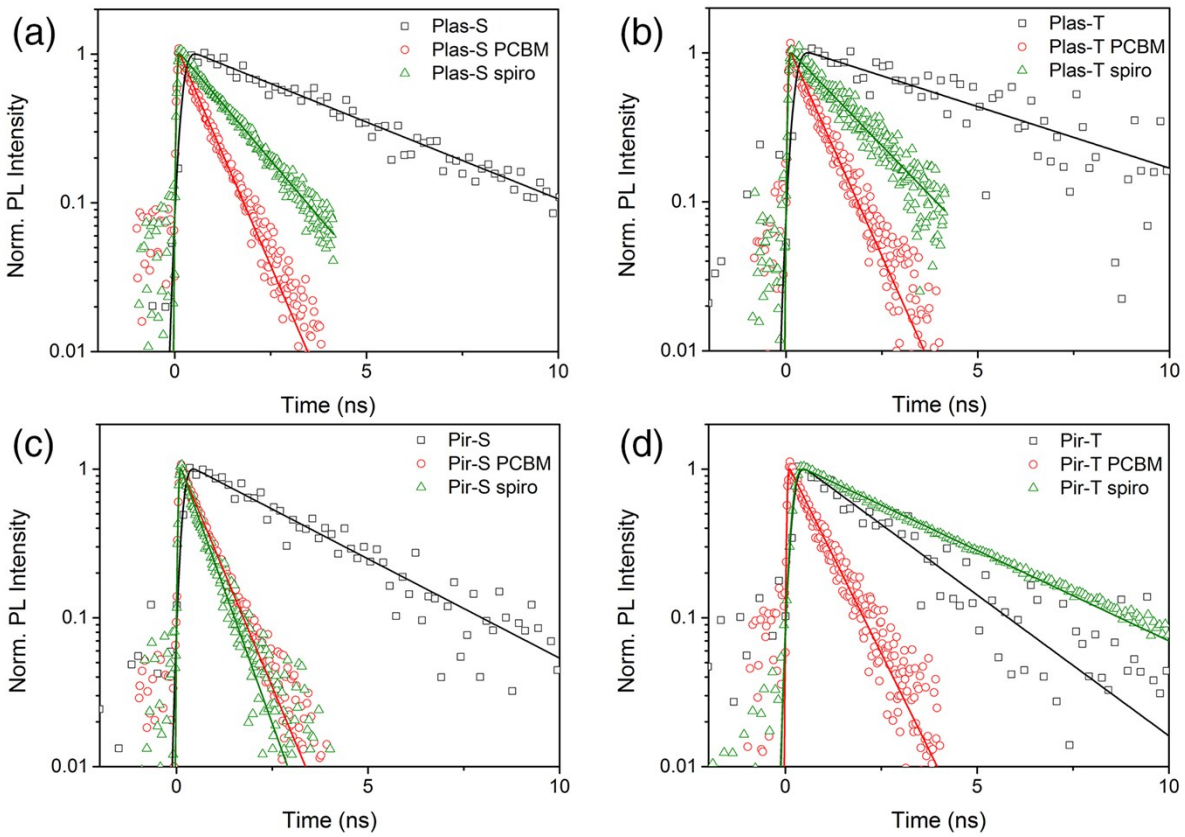

Figure S3. Time-resolved photoluminescence measurements of perovskite films with different treatments (black, squares): (a) Plas-S, (b) Plas-T, (c) Pir-S, and (d) Pir-T and quenching layers, electron quencher PCBM (red, circles) and spiro-OMeTAD (green, upright triangle). Symbols and solid lines represent the derived data and fitted curves, respectively. Note: spiro-OMeTAD was shortened to spiro in the graph for clarity.

Figure S3 shows time-resolved photoluminescence kinetic traces of the perovskite films with different treatments. By using electron (PCBM) and hole quenching (spiro-OMeTAD) layers, the diffusion length can be estimated by using Equation 1 (main text). In all samples except Pir-T/spiro-OMeTAD, the photoluminescence (PL) lifetimes were quenched. Since the PL lifetime in Pir-T/spiro-OMeTAD lengthened with the inclusion of a hole quenching layer, the hole diffusion length could not be estimated in this case.

We derive the equation (Equation 1 in the main text) used to estimate 1D diffusion length within the films by using the equation for the total number of carriers in the active layer, N(t),

$$N(t) = \frac{2n_0 L}{\pi} e^{-\frac{t}{\tau_0}} \sum_{m=0}^{\infty} \frac{(-1)^m \alpha L + \pi\left(m+\frac{1}{2}\right) e^{-\alpha L}}{\left\{\alpha^2 L^2 + \pi^2 \left(m+\frac{1}{2}\right)^2\right\}\left(m+\frac{1}{2}\right)} e^{-\left(m+\frac{1}{2}\right)^2 \frac{\pi^2}{L^2} Dt}$$

where $\tau_0 = 1/k$, is the lifetime of carrier without quenching layer.

We estimate the PL into single exponential decay, and also having the diffusion length $L_D = \sqrt{D\tau_0}$:

$$N(t) = \frac{2n_0 L}{\pi} e^{-\frac{t}{\tau_0}} \sum_{m=0}^{\infty} \frac{(-1)^m \alpha L + \pi\left(m+\frac{1}{2}\right) e^{-\alpha L}}{\left\{\alpha^2 L^2 + \pi^2 \left(m+\frac{1}{2}\right)^2\right\}\left(m+\frac{1}{2}\right)} e^{-\left(m+\frac{1}{2}\right)^2 \pi^2 \left(\frac{L_D}{L}\right)^2 \frac{t}{\tau_0}} \approx A e^{-\frac{t}{\tau_D}}$$

where $A = \int_0^L n_0 e^{-\alpha x} dx = n_0 (1 - e^{-\alpha L})/\alpha$ is the initial concentration. Here, the diffusion length is defined as how far the carrier can travel assuming without the quenching layer and infinite thickness of the active layer. For numerical approximation of the order of error, we used $\alpha L = 0.2$.

$$Ae^{-\frac{t}{\tau_D}} \approx \frac{2n_0 L}{\pi} e^{-\frac{t}{\tau_0}} \left[1.1853 e^{-2.47\left(\frac{L_D}{L}\right)^2 \frac{t}{\tau_0}} + 0.1096 e^{-22.2\left(\frac{L_D}{L}\right)^2 \frac{t}{\tau_0}} + 0.0430 e^{-61}\right.$$

.

As can be seen, for $t > 0$, other than the first term, all other term can be neglected due to very small coefficient and very large decay rate. The approximation of the decay rate therefore:

$$e^{-\frac{t}{\tau_D}} \approx e^{-\left(\frac{1}{\tau_0}+\frac{\pi^2}{4}\left(\frac{L_D}{L}\right)^2\frac{1}{\tau_0}\right)t}$$

$$\frac{t}{\tau_D} = \frac{t}{\tau_0} + \frac{\pi^2}{4}\left(\frac{L_D}{L}\right)^2\frac{t}{\tau_0}$$

$$\frac{\tau_0}{\tau_D} = 1 + \frac{\pi^2}{4}\left(\frac{L_D}{L}\right)^2$$

$$\frac{L_D}{L} = \frac{2}{\pi}\sqrt{\left(\frac{1}{\tau_D/\tau_0} - 1\right)}$$

By substituting the PL lifetimes (τ_D: with quenching layer) and sample thickness, L, into the equation, we can estimate the diffusion length, L_D.

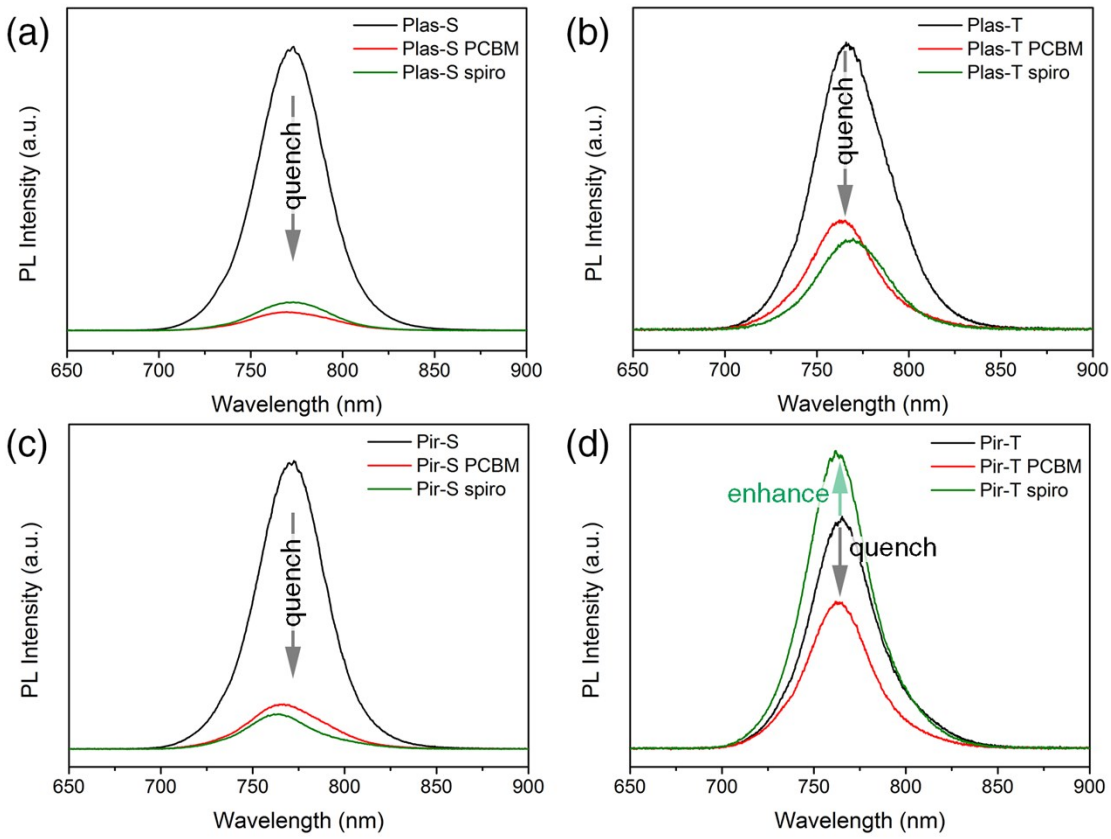

Figure S4. PL quenching observed in the perovskite samples with different treatments (black line) (a) Plas-S, (b) Plas-T, (c) Pir-S, and (d) Pir-T with electron quencher PCBM (red line), and hole quencher spiro-OMeTAD (green line). PL enhancement is observed in Pir-T/spiro-OMeTAD.

Figure S4 shows the steady-state PL of the perovskite films with different treatments. As seen in Figure S4(a-c), the PL is quenched when either electron or hole quenchers (PCBM and spiro-OMeTAD) are present. Together with the results in Figure S3, we conclude that the Fermi level of the perovskite is shifted below that of spiro-OMeTAD's, resulting in poor/no injection into spiro-OMeTAD.

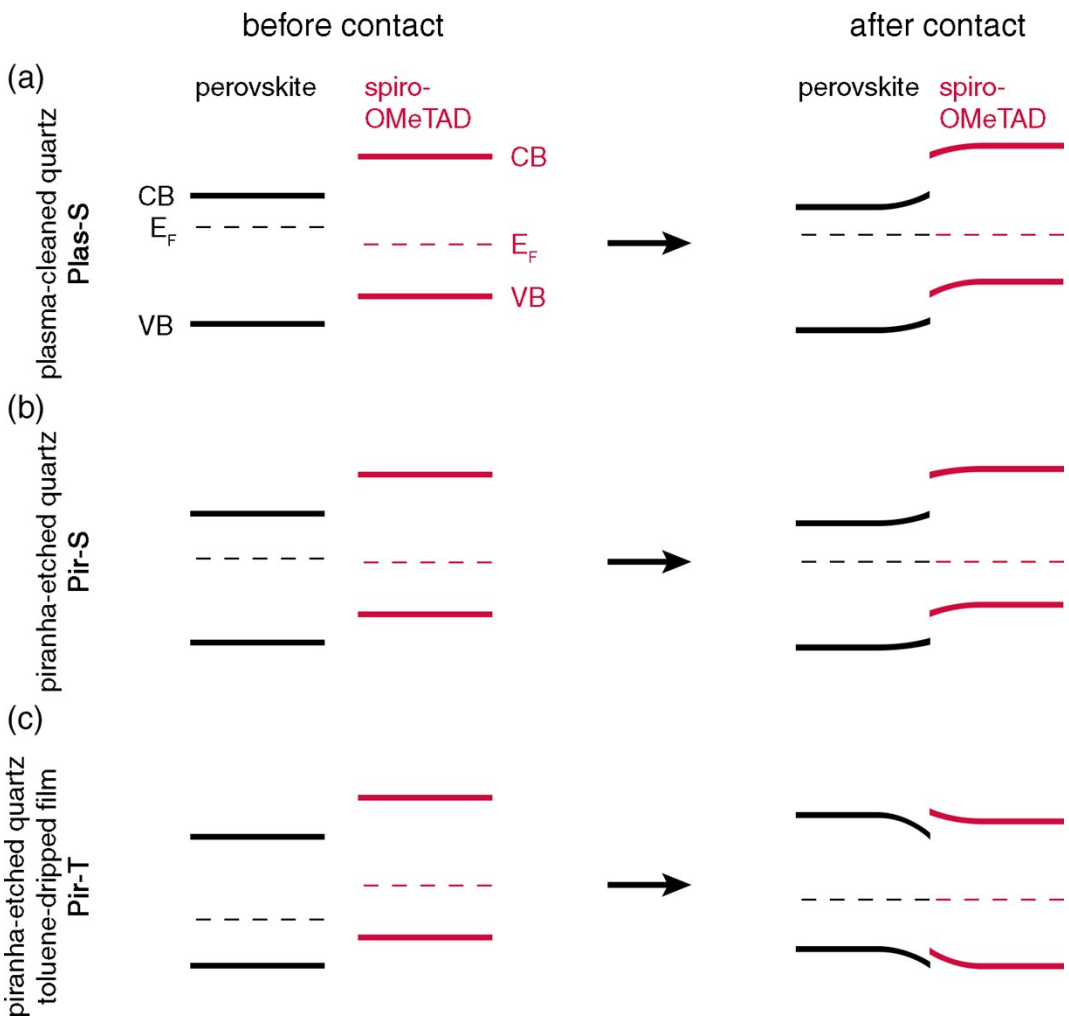

Figure S5. Proposed energetic alignment of $CH_3NH_3PbI_3$ perovskite in contact with spiro-OMeTAD hole quencher after different treatments: (a) Plas-S; (b) Pir-S slightly shifts the perovskite towards more p-type behaviour; and (c) Pir-T that makes the perovskite heavily p-type resulting in poor/no injection of holes with different Fermi level positions of the perovskite film. Energetic alignment of $CH_3NH_3PbI_3$ perovskite having different Fermi level positions of the perovskite film, (a) heavy n-type, (b) n-type, (c) p-type, in contact with spiro-OMeTAD hole quencher. The different doping behavior of the perovskite film may be a consequence of substrate/film treatment.

From the energetics in Figure S5, we see that poor/non-injecting behavior of holes from the perovskite $CH_3NH_3PbI_3$ to spiro-OMeTAD hole quencher is only possible when the Fermi level of

the perovskite is considerably lower than the Fermi level of spiro-OMeTAD, such that an interfacial barrier is formed upon contact. Charge transfer of the holes is possible when the Fermi level of the perovskite is higher, near to, or slightly lower than the Fermi level of the spiro-OMeTAD.

Table S1. Summary of results for the various $CH_3NH_3PbI_3$ samples

Sample	Rq (nm)	Electron diffusion length (nm)	Hole diffusion length (nm)	τ_{PL} (ns)	$\tau_{PL,PCBM}$ (ns)	$\tau_{PL,spiro\text{-}OMeTAD}$ (ps)	TA decay lifetime (ns)
Plas-S	19.5	69.7 ± 0.5	44.3 ± 0.2	4.2 ± 0.1	0.72 ± 0.01	1.43 ± 0.01	8.63 ± 0.08
Plas-T	10.3	78 ± 3	47.8 ± 0.2	5.2 ± 0.2	0.75 ± 0.01	1.63 ± 0.02	9.9 ± 0.2
Pir-S	16.0	60.5 ± 0.7	66.7 ± 0.2	3.3 ± 0.1	0.70 ± 0.01	0.60 ± 0.01	6.95 ± 0.07
Pir-T	16.0	42.2 ± 0.2	--	2.3 ± 0.1	0.83 ± 0.01	3.57 ± 0.01	4.13 ± 0.02

Plas-S, Pir-S: perovskite on plasma-cleaned and piranha-etched substrate, respectively; Plas-T, Pir-T: perovskite on plasma-cleaned and piranha-etched substrate with toluene drip, respectively.